Characterization of collagen formation surrounding osteocytes using second and third harmonic generation

Emily G. Pendleton, Kayvan F. Tehrani, Ruth P. Barrow, Luke J. Mortensen

Emily G. Pendleton, Kayvan F. Tehrani, Ruth P. Barrow, Luke J. Mortensen, "Characterization of collagen formation surrounding osteocytes using second and third harmonic generation," Proc. SPIE 10871, Multimodal Biomedical Imaging XIV, 108710W (27 February 2019); doi: 10.1117/12.2510814

SPIE.

Event: SPIE BiOS, 2019, San Francisco, California, United States

Characterization of Collagen Formation Surrounding Osteocytes using Second and Third Harmonic Generation

Emily G. Pendleton[a], Kayvan F. Tehrani[a], Ruth P. Barrow[a], Luke J. Mortensen*[a,b]
[a]Regenerative Bioscience Center, University of Georgia, 425 River Road, Athens, GA, USA 30601;
[b]School of Chemical, Materials and Biomedical Engineering, University of Georgia, 597 DW Brooks Drive, Athens, GA, USA 30601
*luke.mortensen@uga.edu

ABSTRACT

More than 54 million Americans have or are at high risk of developing a metabolic bone disease; disorders of bone strength that leave individuals with fragile bones and disabilities. The gold standard to evaluate these diseases is dual energy x-ray absorptiometry, but this only measures mineral content. These diseases, however, impact collagen and mineral integrity which impede the bone's ability to store hormones, proteoglycans, and glycoproteins imperative to homeostasis. We have established a second harmonic generation (SHG) polarimetric assay that describes bone collagen organization. To further our analysis, we propose multimodal optical evaluation of bone quality with third harmonic generation (THG) to measure osteocyte dendritic processes. This method of analysis could be used to evaluate the disease state of bone and response to therapy.

Keywords: Second harmonic generation, SHG, Third harmonic generation, THG, bone, polarization, collagen

1. INTRODUCTION

Osteocytes are the most abundant cells in the bone[1]. Osteocytes are formed when osteoblasts, bone-forming cells that secrete collagen and mineral, become trapped in the mineralized extracellular matrix[2]. During this process of terminal differentiation from osteoblast to osteocyte, cells go from a cuboidal shape to a stellate cell with 40-100 dendritic processes, with 50 processes on average[2]. The chemo-regulatory mechanisms that control this transformation are unknown[1] as are the homeostatic implications of the number and length of dendritic processes on the cells[3]. Osteocyte cell bodies reside in lacunae, voids in the collagen matrix with unique collagen fibril organization that are typically 15-20 microns wide[2], and connect to one another and other types of cells via canaliculi, small channels between lacunae that allow for the connection of dendritic processes that form the osteocyte network[3]. Without connections to other cells, osteocytes may succumb to cell death[3]; but while connected, osteocytes regulate the homeostasis of bone.

The osteocyte network regulates the homeostasis of the bone including mineral metabolism[3], response to mechanical forces[1], and remodeling by sending chemical cues to osteoblasts and osteoclasts, bone-absorbing cells[3]. Osteocytes are able to regulate mineral metabolism through DMP-1, PHEX, and FGF-23[4], molecules highly expressed in osteocytes. These osteocyte molecules regulate one another to control the amount of circulating phosphate excreted by the kidneys[3]. Osteocytes have a mechano-sensory function as well. Mechanical loading impacts osteocyte function as well as gene expression[5] and it is known to increase bone mass[6]. Osteocytes inhibit osteoblast formation when they undergo apoptosis by releasing proinflammatory cytokines[7,8] and upregulate the endocytosis of dying osteocytes by osteoclasts, thereby modulating bone resorption processes[9]. Beyond the bone, osteocytes secrete factors that act directly on the kidneys, the heart, the lungs, and blood vessels while impacting the functions of the intestine indirectly[10]. Thus, the osteocyte network has an endocrine function and is critical in maintaining homeostasis in the rest of the body as well.

The lacunocanalicular network not only allows for osteocyte regulation of bone and body homeostasis, but is regulated by osteocytes as well. The surface area of the lacunocanalicular network is many orders of magnitude larger than the surface area of bone[11], thus the removal of a few angstroms of mineral from the surface of the network near each osteocyte would greatly impact the systemic ion levels[3]. Enlarged lacunae have resulted from hibernation[12], space travel[13], and renal osteodystrophy disease[14]. In addition, patients with X-linked hypophosphatemic rickets have had periosteocytic lesions[15]. These morphological changes to the lacunocanalicular network impact the mechano-sensory

Multimodal Biomedical Imaging XIV, edited by Fred S. Azar, Xavier Intes, Qianqian Fang, Proc. of SPIE
Vol. 10871, 108710W · © 2019 SPIE · CCC code: 1605-7422/19/$18 · doi: 10.1117/12.2510814

function of osteocytes and fracture risk[16]. Therefore, understanding both the osteocyte and lacunocanalicular network are important in the understanding of bone homeostasis.

The mature osteocyte and lacunocanalicular network interacts closely with the mineralized collagen fiber mesh network in bone. However, due to challenges in analyzing the bone and osteocyte structure in highly scattering whole bone tissue, osteocyte chemical and metabolic analysis has been largely performed in vitro[1]. The interaction between osteocytes and the lacunocanalicular network has largely been studied ex vivo, visualizing the interaction with confocal or scanning electron microscopy, but typically without integrated analysis of the surrounding matrix[2]. However, the osteocyte responses in vitro lack the natural mechanical matrix deformation of the collagen mesh that is likely to impact osteocyte lacunocanalicular network response[3]. Thus, it is imperative researchers develop methods to analyze the osteocyte and lacunocanicular networks together with the surrounding bone collagen.

Second harmonic generation (SHG) is a non-linear label-free coherent imaging strategy that is useful in describing collagen, a non-centrosymmetric molecule. When high-energy laser pulses interact with collagen molecules that are parallel to the polarization of the excitation beam, the emitted signal is twice the excitation frequency[17]. The induced polarization, P, is dependent on the second order susceptibility tensor, $\chi^{(2)}$, the number of molecules present, N_s, and the average orientation of collagen molecules, $<\beta>$. Thus,

$$P = \chi^{(2)} E^2 \tag{1}$$

and

$$\chi^{(2)} = N_s <\beta> \tag{2}$$

such that when the polarization of the excitation light is aligned with the majority of the collagen molecules, the resulting SHG image is of overall higher intensity when compared to when the polarized light is rotated orthogonally[18]. Conversely, the emitted SHG signal will be of the same intensity regardless of polarization orientation when the collagen molecules are perfectly disorganized. In bone, collagen fiber orientation is heterogeneous. Collagen fibers are organized into lamella sheets, structures roughly 5 microns thick containing fibers oriented in the same direction[19-21], with neighboring lamella sheets are arranged orthogonally to one another. The collagen of muscle, bone, tendon, and skin have been evaluated with SHG using linearly or circularly polarized light[22-24]. However, because the emitted SHG signal is impacted by the highly scattering nature of bone, bone is often sectioned before evaluation and 3-D spatial organization is lost[25].

Third harmonic generation (THG) is a label-free, non-linear imaging strategy that combines the energy of three photons to generate a photon with a wavelength that is one third of the excitation wavelength[26]. Unlike SHG, which is dependent on nonlinear scattering in noncentrosymmetric crystals, THG signal is generated at the interface between two structures with different refractive indices, with a third-order nonlinear susceptibility, $\chi^{(3)}$.[26,27] Therefore, THG is useful at the interface between aqueous interstitial fluids and lipid-rich cell membranes. Various skin cells, the cornea, bones, and muscles have been images with THG to visualize the types of cells present, invasion of disease, and response to therapy[28-33]. Thus, THG and SHG are methods that could be used together to evaluate bone health in vivo to monitor cell health and collagen deposition in diseased states and in response to therapy.

In this work, we find that SHG and THG can be used together to provide understanding of collagen deposition in newly formed bone. We use linearly polarized light rotated over 180^o to describe collagen deposition surrounding the lacunae. We further describe the organization of collagen with gray level co-occurrence matrix (GLCM) measures. THG is useful in the identification of the osteocyte network and the connections made by individual osteocytes. This implementation of SHG and THG analysis could be used as a guide for researchers in bone health to describe the lacunocanalicular network and osteocyte health.

2. METHODOLOGY

2.1 Animals

The use and experimentation upon all animals in this study was approved by The University of Georgia Institutional Animal Care and Use Committee. Wild type B6/129 mice were sacrificed at two weeks of age. The skulls

were skinned and embedded with dental cement to prevent movement. The calvaria bones were stored at -20°C and hydrated with PBS during imaging.

2.2 Optical setup

The optical setup for imaging experiments used a two-photon microscope described in our previous efforts.[34] The optical setup consists of a Ti:Sapphire ultrafast laser (Chameleon ultra II) that produces light from 680nm to 1080nm. We adjust the group velocity dispersion to shorten the pulses and maximize the THG signal intensity. The epi-detected second harmonic generation (SHG) signal of collagen was collected with a PMT (Hamamatsu) and a 525/50 bandpass filter while the back-propagated Third Harmonic Generation (THG) signal of osteocytes was collected with a PMT and a 356/30 bandpass filter.

2.3 Data analysis: collagen texture

Both ImageJ 1.50e (Wayne Rasband, National Institute of Heath, USA) and MatLab (Matlab and Statistics Toolbox Release R2017a, The MathWorks Inc., Natick, MA, USA) were used to analyze SHG image stacks containing angle-encoded information to visualize collagen orientation. Color images were formed with each stack normalized to the maximum intensity. Images were normalized to the reciprocal of a standard set of CFSE images and every 10° of polarized light was assigned a different color. To describe the orientation and organization of the collagen lamella sheets, the final color-coded image was created by selecting the maximum intensity of each colored pixel.

In order to quantify the variation of collagen orientation seen, we used the gray-level co-occurrence matrix (GLCM). The GLCM is a spatial statistical method that compares how often different combinations of gray-level intensities occur within an image. The matrix is made when the pixel of interest is compared to its neighbors at 0°, 45°, 90°, and135° within a defined neighborhood of pixels. We defined this neighborhood as 50 pixels (6.9 μm) and examined the homogeneity, correlation, energy, and contrast. Each parameter was defined as:

$$\text{Homogeneity} = \Sigma\, p(i,j) / [1 + |i-j|] \tag{3}$$

$$\text{Correlation} = \Sigma\, [(i-\mu_i)(j-\mu_j)p(i,j) / \sigma_i\sigma_j \tag{4}$$

$$\text{Energy} = \Sigma\, p(i,j)^2 \tag{5}$$

$$\text{Contrast} = \Sigma\, |i-j|^2\, p(i,j) \tag{6}$$

Where *i* is the gray level of interest, *j* is the gray level being compared, *p(i,j)* is the number of times that gray-level pair occurs in the image, and μ is the mean while σ is the standard deviation of the overall GLCM. A total of 20 gray levels were used for analysis. Matlab software was used to compute all values.

2.4 Data analysis: lacunae

Osteocyte lacunae were visualized with Matlab by exploiting the voids of the SHG images. A 3-D minimum filter (σ = 2) was applied and followed by a 3-D Gaussian filter (σ = 1.5). A 3-D adaptive threshold was applied to each stack. Holes in the binary images were filled and only objects larger than 1,400 microns^3 were permitted to pass and be viewed.

2.5 Data analysis: osteocytes

Osteocytes were visualized and analyzed with ImageJ. The original THG image was processed by removing bright outliers, applying a 3-D Gaussian filter (σ = 1.0), and an adaptive threshold was applied before a final smoothing. Objects larger than 27 microns^3 were permitted to pass and be viewed.

3. RESULTS

3.1 Collagen texture

The calvaria of a mouse was imaged using a two-photon microscope and rotated linearly polarized light at each depth. Each angle of light was assigned a color and a maximum projection image was formed (Figure 1A). The projection allows us to see aligned lamella sheets. Stacked and neighboring lamella sheets have opposing colors, indicating that the collagen fibers that compose those sheets have roughly orthogonal orientations.

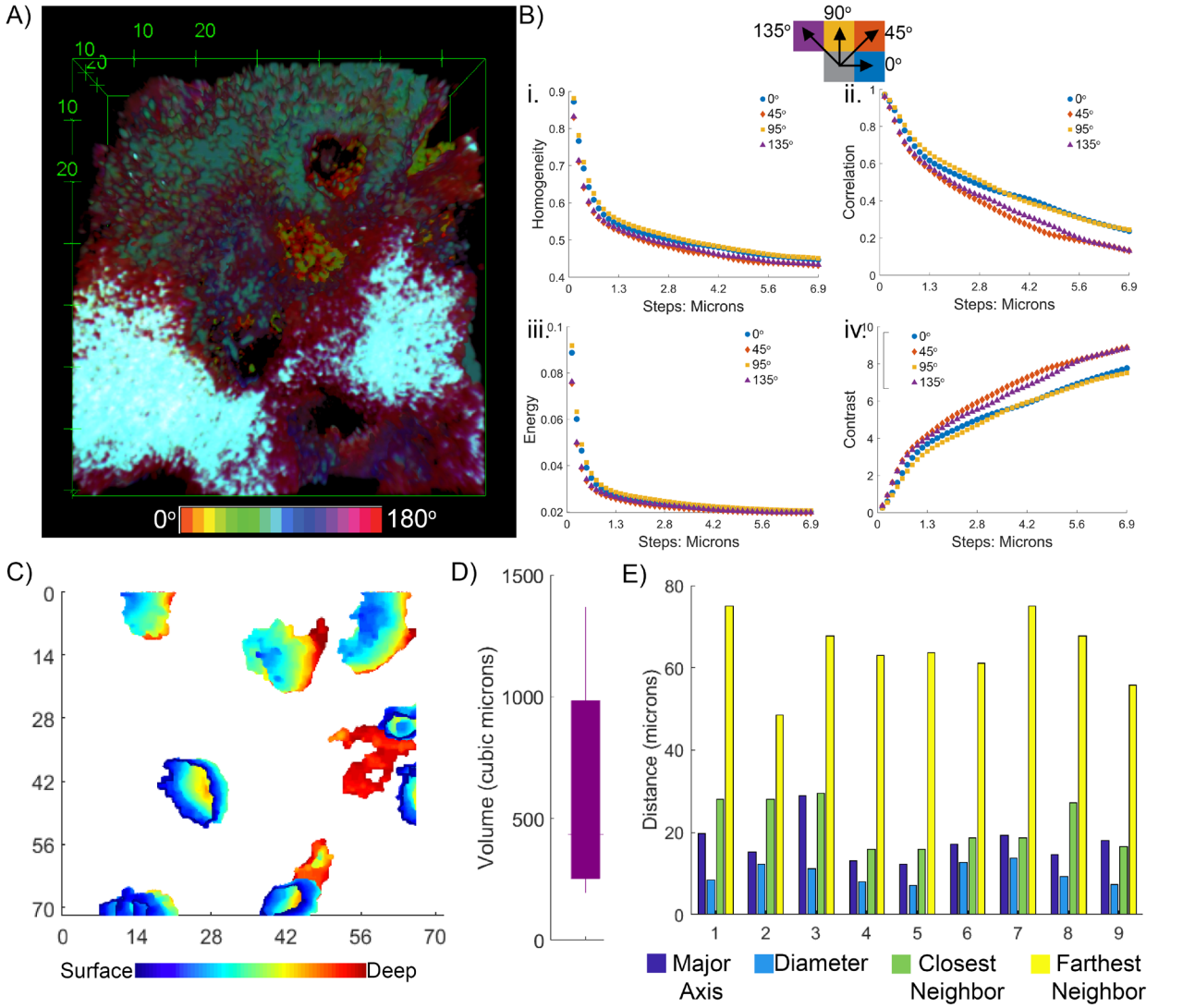

Figure 1. Second Harmonic Generation allows for collagen and lacunae analysis. (A) 3-D SHG image obtained using linearly polarized light depicts the formation of lamella sheets. (B) Analyzing the collagen fibers that compose the lamella sheets with GLCM describes the texture of the collagen fibers. (C) Analyzing the voids of the SHG image allows for the 3-D reconstruction of osteocyte lacunae. (D-E) The parameters of the osteocyte lacunae can be quantified.

The collagen texture of lamella sheets can be described with the GLCM. To do so, we used and SHG projection of the average of all angles of polarized light capturing bone 5 microns from the surface. Lacunae were omitted with an Otsu threshold and not considered in this analysis. Homogeneity describes how similar the gray levels are to one another within a given image, with values close to 1 indicating like gray values and values of 0 indicating dissimilar gray values. Here, when comparing pixels at all angles (0° – 135°) the homogeneity factor indicates similar gray levels for all

neighboring pixels within the first micron (Figure 1B(i)). Likely, these pixels are within the same collagen fiber. As the neighborhood is expanded to nearly 7 microns, the homogeneity drops to 0.4.

Similar to homogeneity, correlation determines similarities between pixels of interest while accounting for the mean of the image, thus it determines how dependent pairs of gray levels are on one another. Perfectly negatively or positively correlated images have values of -1 or 1, with a constant image having a value of NaN. The correlation of this SHG image indicates that similar gray levels are found within the first micron of neighbors (Figure 1B(ii)), but the intensity of pixels that are near 7 microns away are not well correlated to one another.

The energy parameter of a GLCM describes the orderliness or uniformity among neighboring pixels, with values ranging from [0 1]; 1 indicates a constant image. The energy of our SHG image is very low even when examining neighbors that would likely be within the same collagen fiber (Figure 1B(iii)).

Finally, we examined the contrast of the image using the GLCM, describing the sum of square variance, with a range of [0 ((number of gray levels)-1)^2]. Here, a value of 0 indicates a constant image. We see low contrast values when we examine pixels within the first micron, indicating similar gray levels, but again we see a sharp increase in the contrast when we move farther away from the pixel of interest, indicating dissimilar gray values (Figure 1B(iv)).

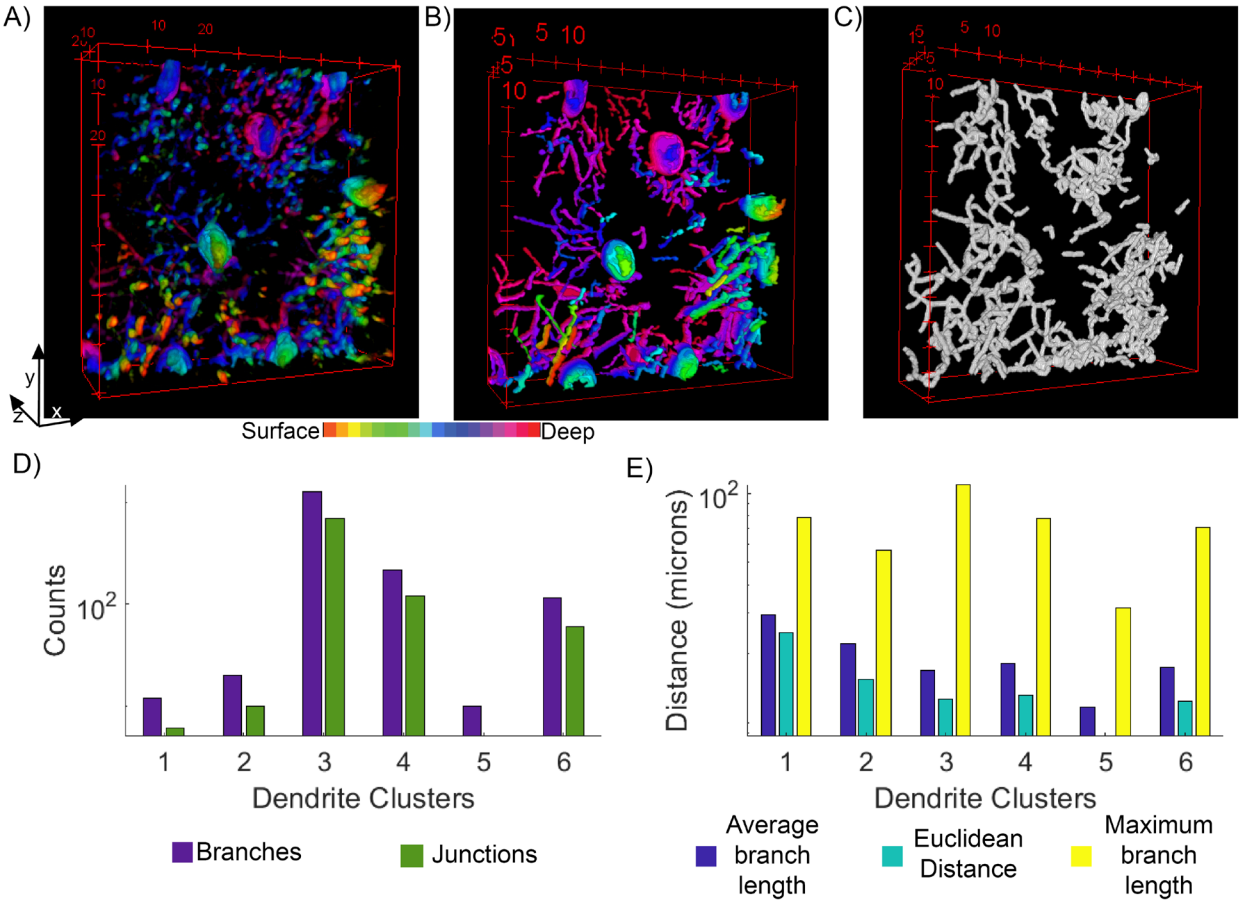

Figure 2. THG images of visualize osteocytes and permit quantification. (A) The 3-D THG image of osteocytes was reconstructed with color indicating depth of feature. (B) The resultant processed THG image that is used for segmentation. (C) The segmented dendrites of the osteocytes. (D-E) The properties of dendrites can be quantified to measure average and maximum branch length, Euclidean distance, as well as number of branches and junctions.

3.2 Lacunae

The absence of SHG signal indicates a lack of collagen. Here, we are able to visualize these gaps, lacunae, where osteocytes reside (Figure 1C). With segmentation, we can identify individual lacunae and describe them. On average, the lacunae have a volume of 618 microns^3. Parameters such as the major axis length (17.5 ± 5.0 microns),

diameter (10.0 ± 2.5 microns) and proximity of lacunae (nearest: 22.0 ± 6.0 microns; farthest: 64.2 ± 8.6 microns) can also be determined (Figure 1-D-E). Values given are the average and standard deviation of 9 lacunae.

3.3 Osteocytes

THG is able to identify osteocyte bodies and dendrites due to the difference in refractive index between the cell and the surrounding interstitial fluid. First, we visualized osteocytes with a 3-D reconstruction, color coded by depth (Figure 2A). Next, to describe osteocytes, we needed to process the image to allow for segmentation (Figure 2B). Finally, by skeletonizing the image, we can visualize the dendrites of the osteocytes (Figure 2C). The resulting skeletonized image allows for quantification of average branch length (19.3 ± 6.0 microns), Euclidean distance (15.5 ± 5.4 microns), number of branches (206 ± 436), number of junctions (112 ± 238), and the longest connection of dendrites (70.8 ± 25.9 microns) (Figure 3D-E).

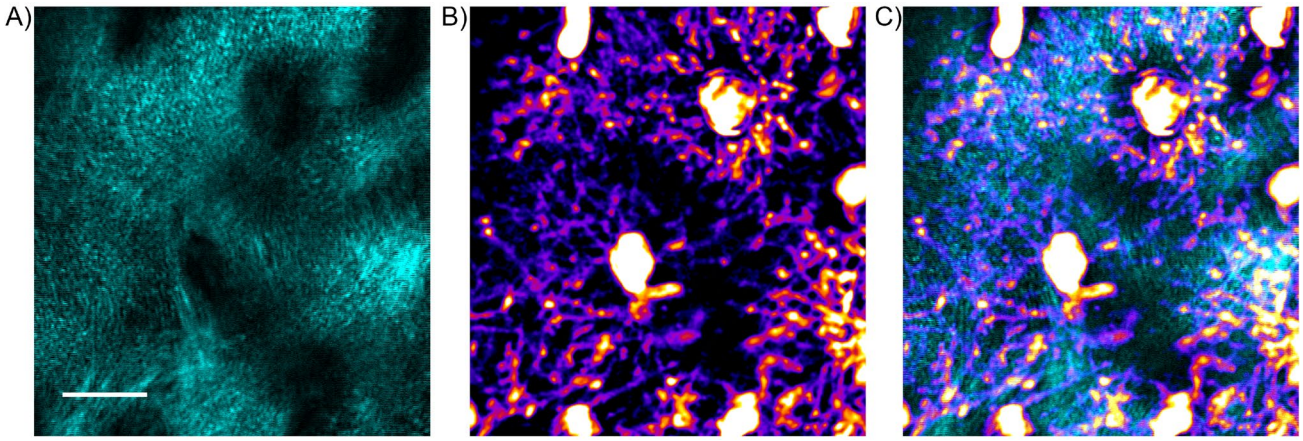

Figure 3. SHG and THG methods provide complimentary information about bone health. (A) SHG projection of lamella sheets. (B) THG projection of osteocytes. (C) Merge of SHG and THG images. Scale bar 15 microns.

4. DISCUSSION

This paper demonstrates how SHG methods of collagen analysis can be used together with THG analysis of osteocytes (Figure 3). SHG analysis is critical to understanding how collagen fibers are oriented. Disruption to the layering of collagen fibers can be indicative of disease state. This method of analysis can evaluate how disease responds to therapy. By incorporating the statistical method of analyzing the texture of collagen with GLCM, these SHG images can be analyzed. Here, we visualized collagen sheets represented by different colors. Our GLCM results indicated that gray levels of the pixel of interest were like neighbors within 1 micron. Past 1 micron, the GLCM demonstrated that the gray levels became different from their neighbors. This indicates collagen molecules within a given fiber share similar intensities. It is possible that overall lamellar regions are brightest at a given angle of polarized light, the intensity of the light generated among neighboring, aligned collagen fibers may be different. Further analysis of the GLCM using images from one angle of linearly polarized light may elucidate these findings. This work should also be carried out on different types of bone. Here, we used juvenile bone that is undergoing extensive remodeling. The transformative nature of this bone may be contributing to the empirical GLCM results. Our lacunae data showed consistent measurements of lacunae within the field of view, with standard deviations among the group never surpassing 30%. Future work is needed to determine baseline lacunae and GLCM measures for different types of bone at various stages of development.

Osteocyte health is critical to bone homeostasis, but due to their location intertwined in collagen, osteocytes have been difficult to study. Here we demonstrate quantifiable measures that can obtained from THG images of osteocytes. As expected, the average branch length, maximum branch length, and Euclidean distance of the dendrite clusters were positively correlated with one another. In addition, more branching of dendrites also indicated that more junctions among dendrites would occur. Like the SHG measurements, more bone samples need to be examined to determine the homeostatic baseline for these measures. One of the dendrite clusters that we measured had considerably more dendrites than the others. When visually examining the clusters of dendrites, this large cluster consists of dendrites originating from several cells. Moving forward, it will be important to separate these dendrites and identify the origins

and synapses of the dendrites. Improving this segmentation will help determine how the number of dendrites on an osteocyte impact bone health.

The work in this manuscript demonstrates the integration of quantifiable SHG and THG imaging for bone health analysis and seeks to serve as a basis of investigation for other researchers.

REFERENCES

1 *Dynamics of Bone and Cartilage Metabolism: Principles and Clinical Applications*. 2nd Edition edn, (Academic Press, 2006).

2 Chen, H., Senda, T. & Kubo, K.-y. The osteocyte plays multiple roles in bone remodeling and mineral homeostasis. *Medical Molecular Morphology* **48**, 61-68, doi:10.1007/s00795-015-0099-y (2015).

3 Bonewald, L. F. The amazing osteocyte. *Journal of bone and mineral research : the official journal of the American Society for Bone and Mineral Research* **26**, 229-238, doi:10.1002/jbmr.320 (2011).

4 Bonewald, L. F. Osteocytes as dynamic multifunctional cells. *Ann N Y Acad Sci* **1116**, 281-290, doi:10.1196/annals.1402.018 (2007).

5 Robling, A. G. *et al.* Mechanical stimulation of bone in vivo reduces osteocyte expression of Sost/sclerostin. *J Biol Chem* **283**, 5866-5875, doi:10.1074/jbc.M705092200 (2008).

6 Rubin, C. T. Skeletal strain and the functional significance of bone architecture. *Calcif Tissue Int* **36 Suppl 1**, S11-18 (1984).

7 Lacey, D. C., Simmons, P. J., Graves, S. E. & Hamilton, J. A. Proinflammatory cytokines inhibit osteogenic differentiation from stem cells: implications for bone repair during inflammation. *Osteoarthritis Cartilage* **17**, 735-742, doi:10.1016/j.joca.2008.11.011 (2009).

8 Yang, J. *et al.* HMGB1 is a bone-active cytokine. *J Cell Physiol* **214**, 730-739, doi:10.1002/jcp.21268 (2008).

9 Cerri, P. S., Boabaid, F. & Katchburian, E. Combined TUNEL and TRAP methods suggest that apoptotic bone cells are inside vacuoles of alveolar bone osteoclasts in young rats. *J Periodontal Res* **38**, 223-226 (2003).

10 Dallas, S. L., Prideaux, M. & Bonewald, L. F. The osteocyte: an endocrine cell ... and more. *Endocr Rev* **34**, 658-690, doi:10.1210/er.2012-1026 (2013).

11 Marotti, G., Ferretti, M., Remaggi, F. & Palumbo, C. Quantitative evaluation on osteocyte canalicular density in human secondary osteons. *Bone* **16**, 125-128 (1995).

12 Haller, A. C. & Zimny, M. L. Effects of hibernation on interradicular alveolar bone. *J Dent Res* **56**, 1552-1557, doi:10.1177/00220345770560122601 (1977).

13 Iagodovskii, V. S., Triftanidi, L. A. & Gorokhova, G. P. [Effect of space flight on rat skeletal bones (an optical light and electron microscopic study)]. *Kosm Biol Aviakosm Med* **11**, 14-20 (1977).

14 Bonucci, E. *et al.* [Clinico-morphological correlations in uremic osteodystrophy of patients with conservative and hemodialytic treatment with special regard to the ultrastructure]. *Minerva Nefrol* **22**, 99-108 (1975).

15 Marie, P. J. & Glorieux, F. H. Relation between hypomineralized periosteocytic lesions and bone mineralization in vitamin D-resistant rickets. *Calcif Tissue Int* **35**, 443-448 (1983).

16 Nicolella, D. P., Moravits, D. E., Gale, A. M., Bonewald, L. F. & Lankford, J. Osteocyte lacunae tissue strain in cortical bone. *Journal of biomechanics* **39**, 1735-1743, doi:10.1016/j.jbiomech.2005.04.032 (2006).

17 Cox, G. *et al.* 3-dimensional imaging of collagen using second harmonic generation. *J Struct Biol* **141**, 53-62 (2003).

18 Campagnola, P. J. & Loew, L. M. Second-harmonic imaging microscopy for visualizing biomolecular arrays in cells, tissues and organisms. *Nat Biotechnol* **21**, 1356-1360, doi:10.1038/nbt894 (2003).

19 Weiner, S., Traub, W. & Wagner, H. D. Lamellar bone: structure-function relations. *J Struct Biol* **126**, 241-255, doi:10.1006/jsbi.1999.4107 (1999).

20 Genthial, R. *et al.* Label-free imaging of bone multiscale porosity and interfaces using third-harmonic generation microscopy. *Scientific Reports* **7**, 3419, doi:10.1038/s41598-017-03548-5 (2017).

21 Rho, J. Y., Kuhn-Spearing, L. & Zioupos, P. Mechanical properties and the hierarchical structure of bone. *Med Eng Phys* **20**, 92-102 (1998).

22 Lee, W., Rahman, H., Kersh, M. E. & Toussaint, K. C., Jr. Application of quantitative second-harmonic generation microscopy to posterior cruciate ligament for crimp analysis studies. *J Biomed Opt* **22**, 46009, doi:10.1117/1.jbo.22.4.046009 (2017).

23 Yasui, T., Tohno, Y. & Araki, T. Determination of collagen fiber orientation in human tissue by use of polarization measurement of molecular second-harmonic-generation light. *Appl Opt* **43**, 2861-2867 (2004).
24 Campagnola, P. J. *et al.* Three-dimensional high-resolution second-harmonic generation imaging of endogenous structural proteins in biological tissues. *Biophys J* **82**, 493-508, doi:10.1016/s0006-3495(02)75414-3 (2002).
25 Campagnola, P. Second Harmonic Generation Imaging Microscopy: Applications to Diseases Diagnostics. *Analytical chemistry* **83**, 3224-3231, doi:10.1021/ac1032325 (2011).
26 Barad, Y., Eisenberg, H., Horowitz, M. & Silberberg, Y. Nonlinear scanning laser microscopy by third harmonic generation. *Applied Physics Letters* **70**, 922-924, doi:10.1063/1.118442 (1997).
27 Müller, Squier, Wilson & Brakenhoff. 3D microscopy of transparent objects using third-harmonic generation. *Journal of Microscopy* **191**, 266-274, doi:10.1046/j.1365-2818.1998.00399.x (1998).
28 Tai, S.-P. *et al.* Optical biopsy of fixed human skin with backward-collected optical harmonics signals. *Optics Express* **13**, 8231-8242, doi:10.1364/OPEX.13.008231 (2005).
29 Weigelin, B., Bakker, G.-J. & Friedl, P. Intravital third harmonic generation microscopy of collective melanoma cell invasion. *IntraVital* **1**, 32-43, doi:10.4161/intv.21223 (2012).
30 Aptel, F. *et al.* Multimodal Nonlinear Imaging of the Human Cornea. *Investigative Ophthalmology & Visual Science* **51**, 2459-2465, doi:10.1167/iovs.09-4586 (2010).
31 Olivier, N., Aptel, F., Plamann, K., Schanne-Klein, M.-C. & Beaurepaire, E. Harmonic microscopy of isotropic and anisotropic microstructure of the human cornea. *Optics Express* **18**, 5028-5040, doi:10.1364/OE.18.005028 (2010).
32 Rehberg, M., Krombach, F., Pohl, U. & Dietzel, S. Label-Free 3D Visualization of Cellular and Tissue Structures in Intact Muscle with Second and Third Harmonic Generation Microscopy. *PLOS ONE* **6**, e28237, doi:10.1371/journal.pone.0028237 (2011).
33 Tokarz, D. *et al.* Intravital imaging of osteocytes in mouse calvaria using third harmonic generation microscopy. *PLoS One* **12**, e0186846, doi:10.1371/journal.pone.0186846 (2017).
34 Tehrani, K. F., Kner, P. & Mortensen, L. J. 10 (SPIE).